



Modeling the Ring Current and its Response to Solar Wind Conditions

Kristi A. Keller, Ayrís Falasca, Mei-Ching Fok, Michael
Hesse, Lutz Rastaetter, Maria M. Kuznetsova
Goddard Space Flight Center

Tamas I. Gombosi, Darren L. DeZeeuw
University of Michigan



Abstract

Magnetospheric storms and substorms can enhance the ring current. This enhancement causes a reduction of the magnetic field at the Earth's surface at mid- and low-latitudes that can be measured by the Dst index. Using a combination of the University of Michigan's BATSRUS code and Mei-Ching Fok's Kinetic Ring Current model we will study how different real and simulated solar wind conditions impact the modeled ring current's energy and correlate this with changes in recorded Dst. We will also explore the relative importance of the ionospheric electric field driver and changes in the magnetic field on the evolution of the ring current. Additionally, we will compare proton fluxes from our simulation to fluxes measure by geosynchronous satellites.

BATSRUS Information

- BATSRUS solves the ideal MHD equations using an adaptive mesh. In this run the smallest resolution was $1/8 R_E$. After the initial setup, the grid was fixed.
- The box was from -255 to $33 R_E$ in the GSM x direction and -48 to $48 R_E$ in the other two directions.
- We used level 2 ACE data and propagated the solar wind data from ACE to $33 R_E$ using an average velocity.
- The FACs at $4 R_E$ are mapped along dipole field lines to the ionosphere to calculate the electrostatic potential in the ionosphere.

Fok Model

- The Fok Ring Current Model calculates the evolution of the ring current particle fluxes by solving a bounce-averaged Boltzmann transport equation.
- The model uses a combined convection-diffusion approach included drift, charge exchange, radial and pitch angle diffusion.
- The Fok Ring Current Model uses the ionospheric potential and magnetic field from the BATSRUS model.
- The Fok Ring Current Model uses the density and temperature from the BATSRUS model at the Ring Current Model's outer boundary.

May 23, 2002

Solar Wind Data Propagated to $x = 33 R_E$

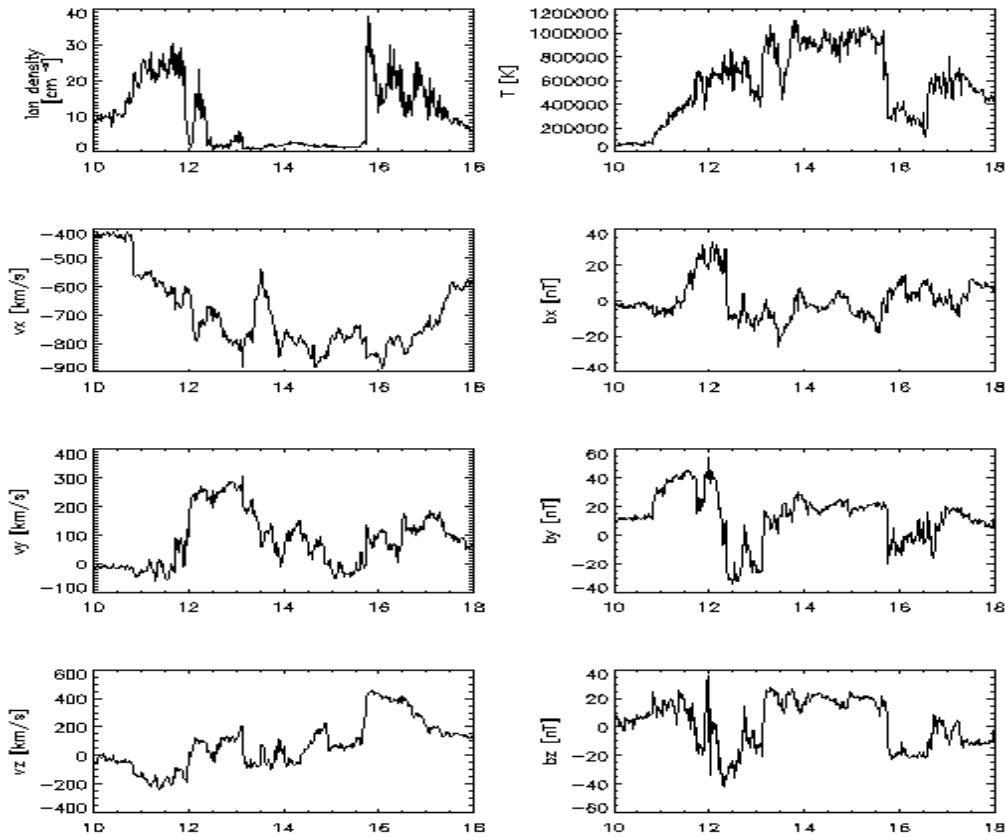


Figure 1

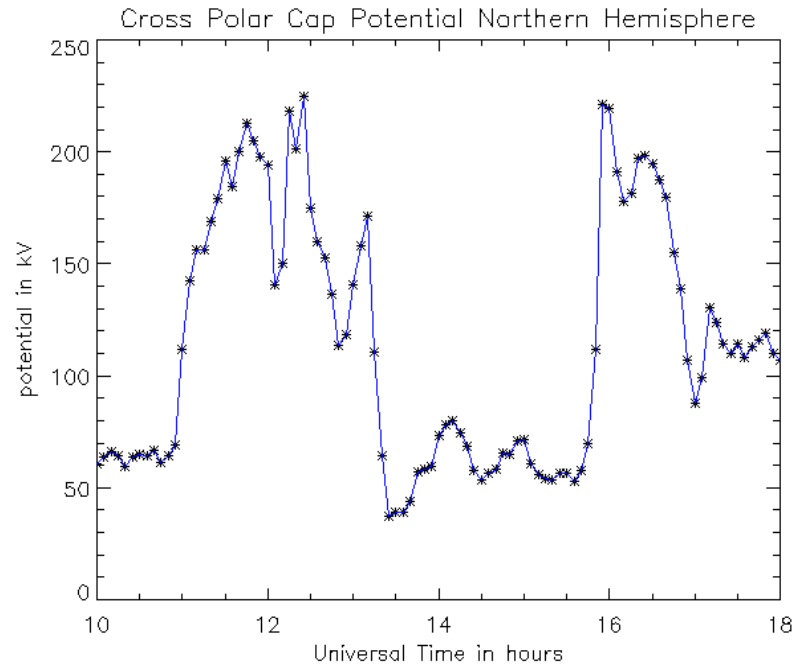


Figure 2

Ring Current (210 keV)

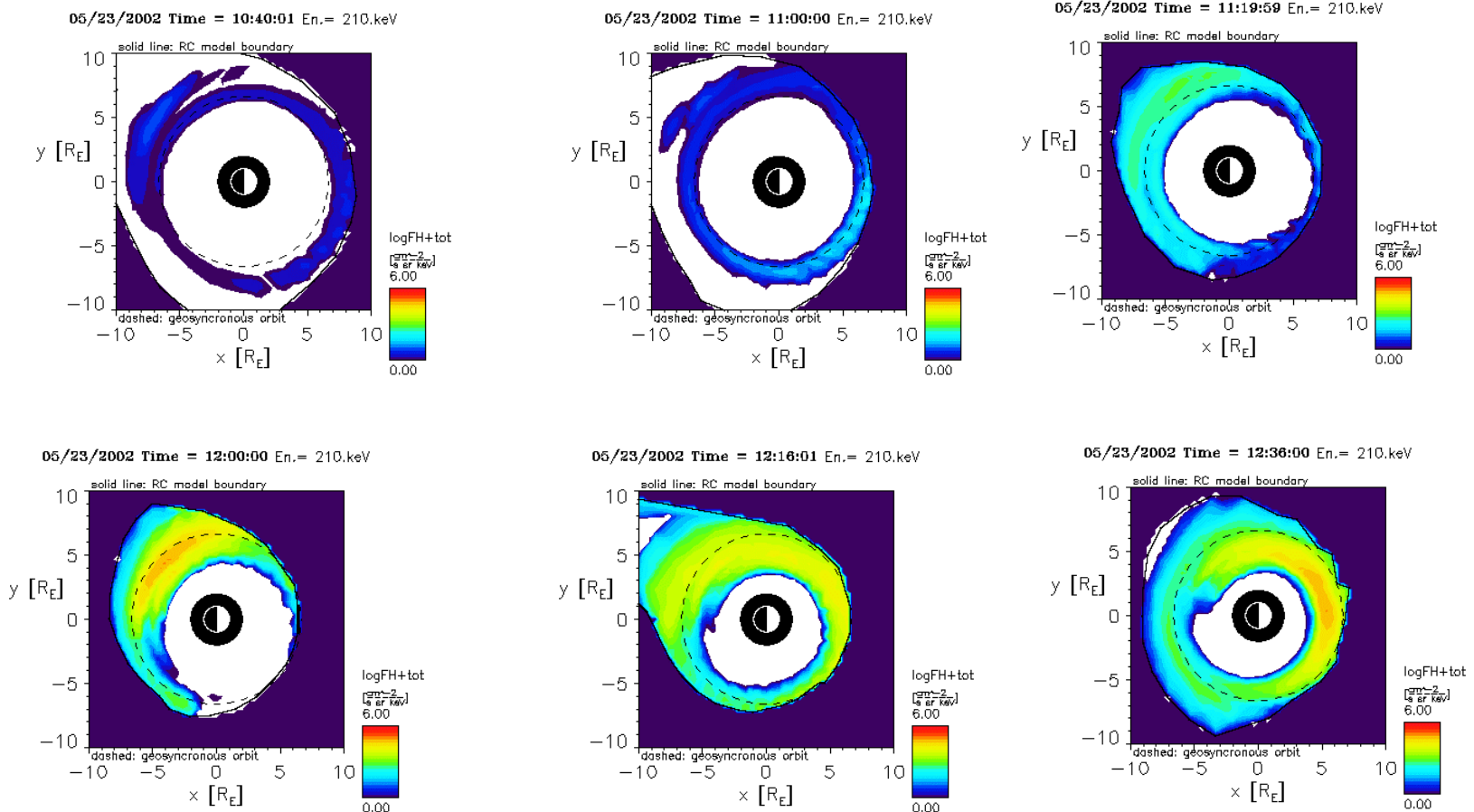


Figure 3

Ring Current (210 keV)

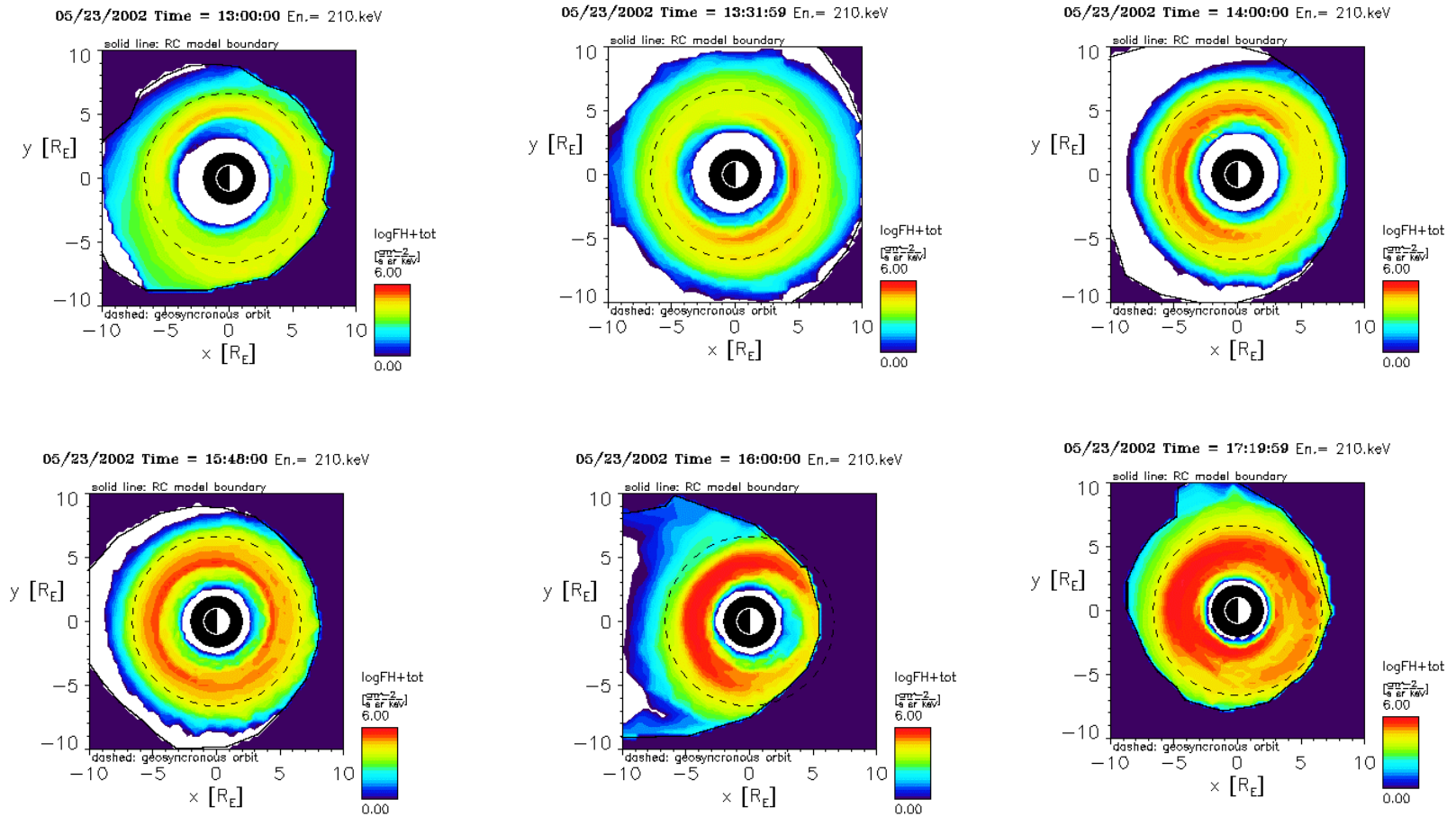


Figure 4

Ring Current (100 keV)

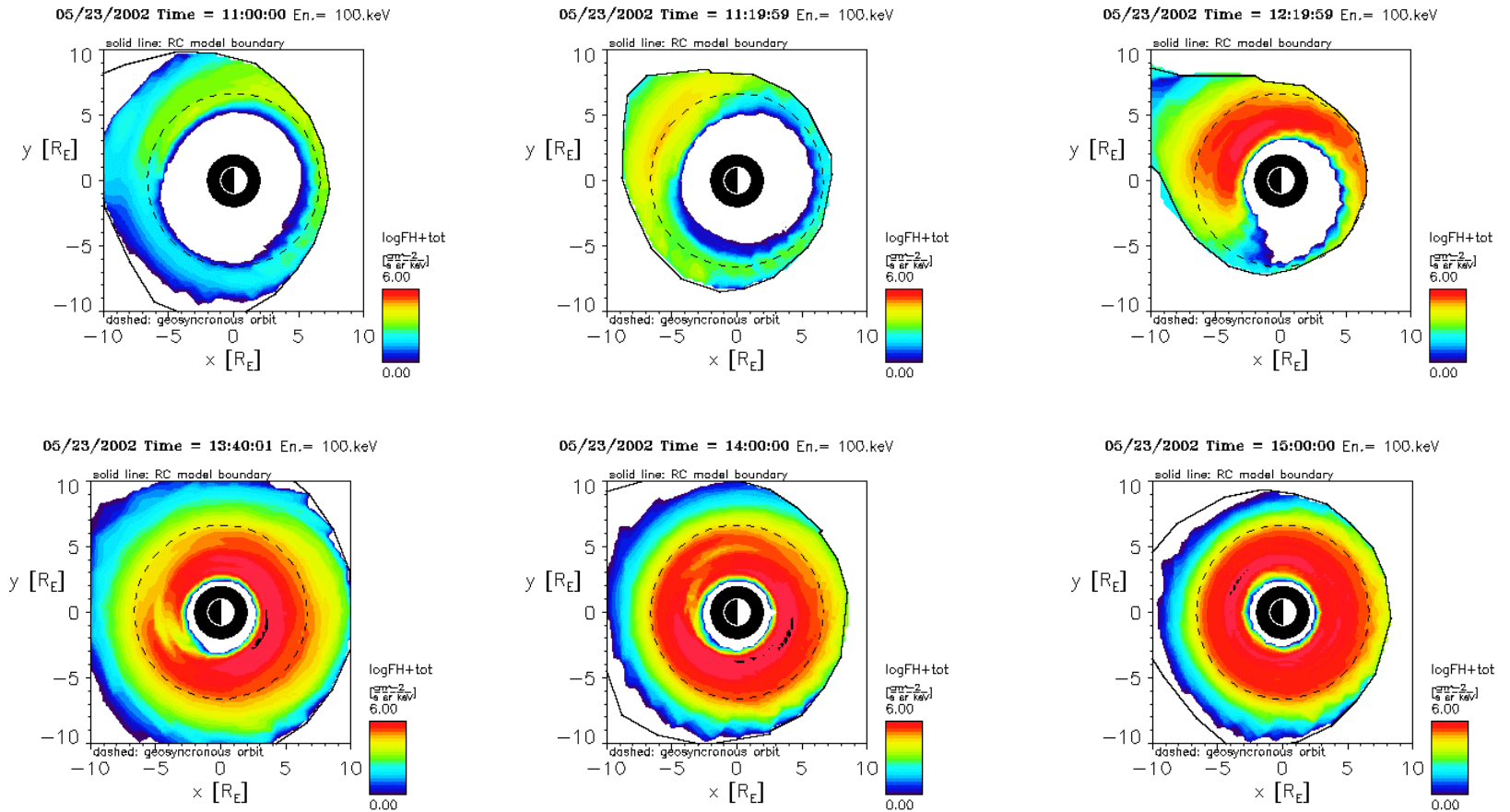
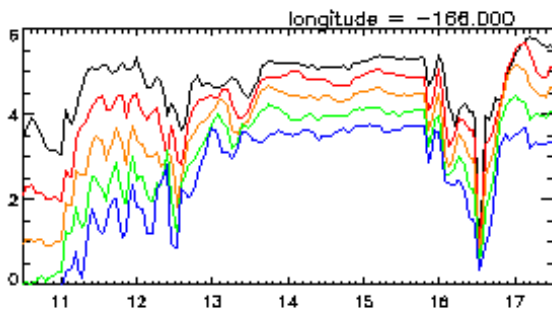
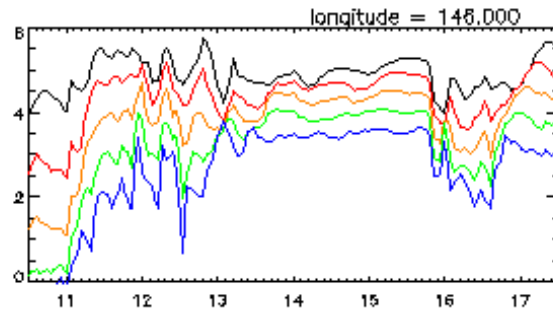
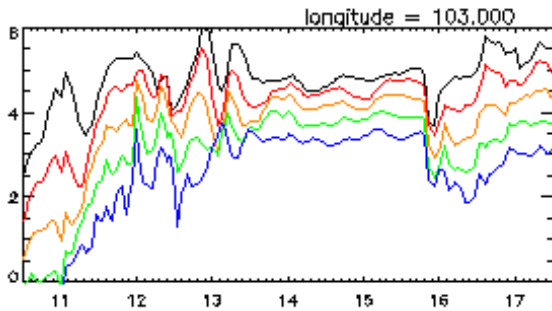
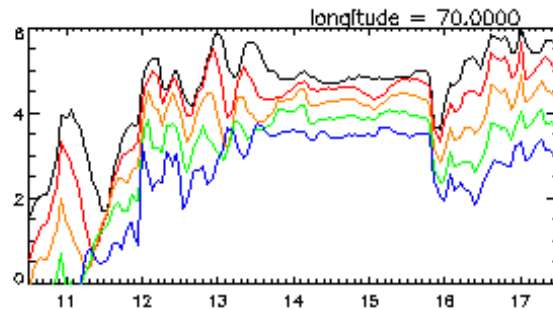
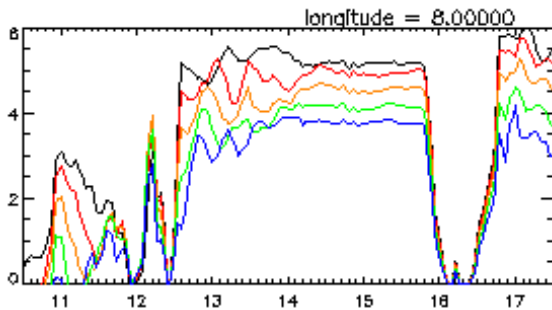


Figure 5

Model Proton Flux

Log(Pitch Angle-Averaged
Differential Flux ($\#/cm^2/s/sr/keV$))



Universal Time (Hours)

May 23

Figure 6

Energies (keV):

62.5 black

94 red

141.5 orange

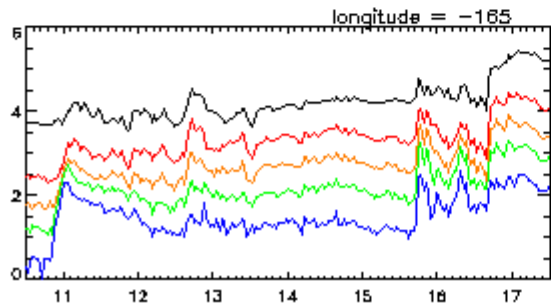
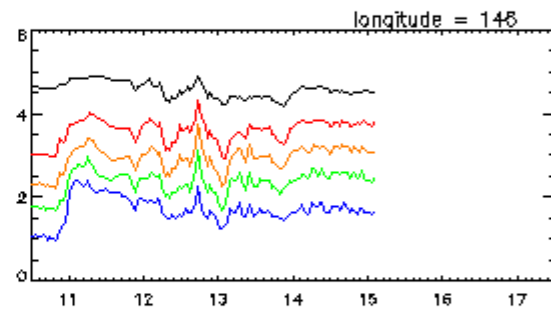
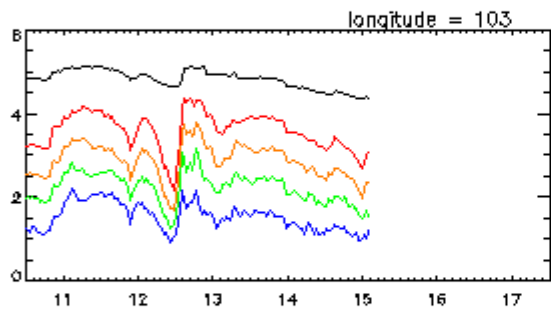
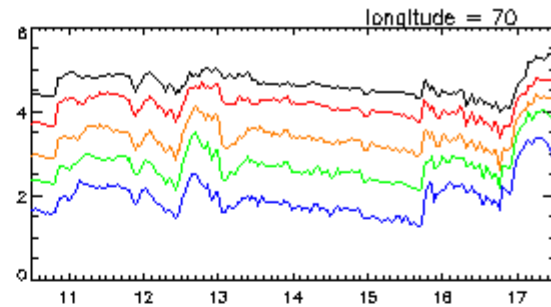
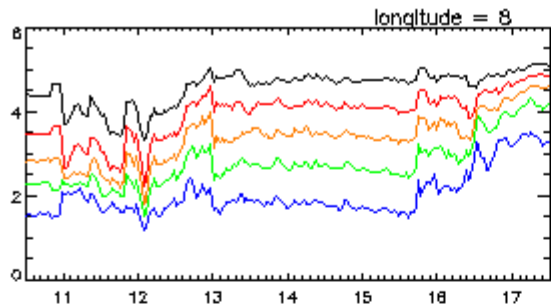
210 green

300 blue

Universal Time (Hours)

LANL Geosynchronous Proton Data

Log(Pitch Angle-Averaged
Differential Flux ($\#/cm^2/s/sr/keV$))



Universal Time (Hours)

May 23

Figure 7

Energies (keV):

50-75 black

75-113 red

113-170 orange

170-250 green

250-400 blue

Magnetosphere

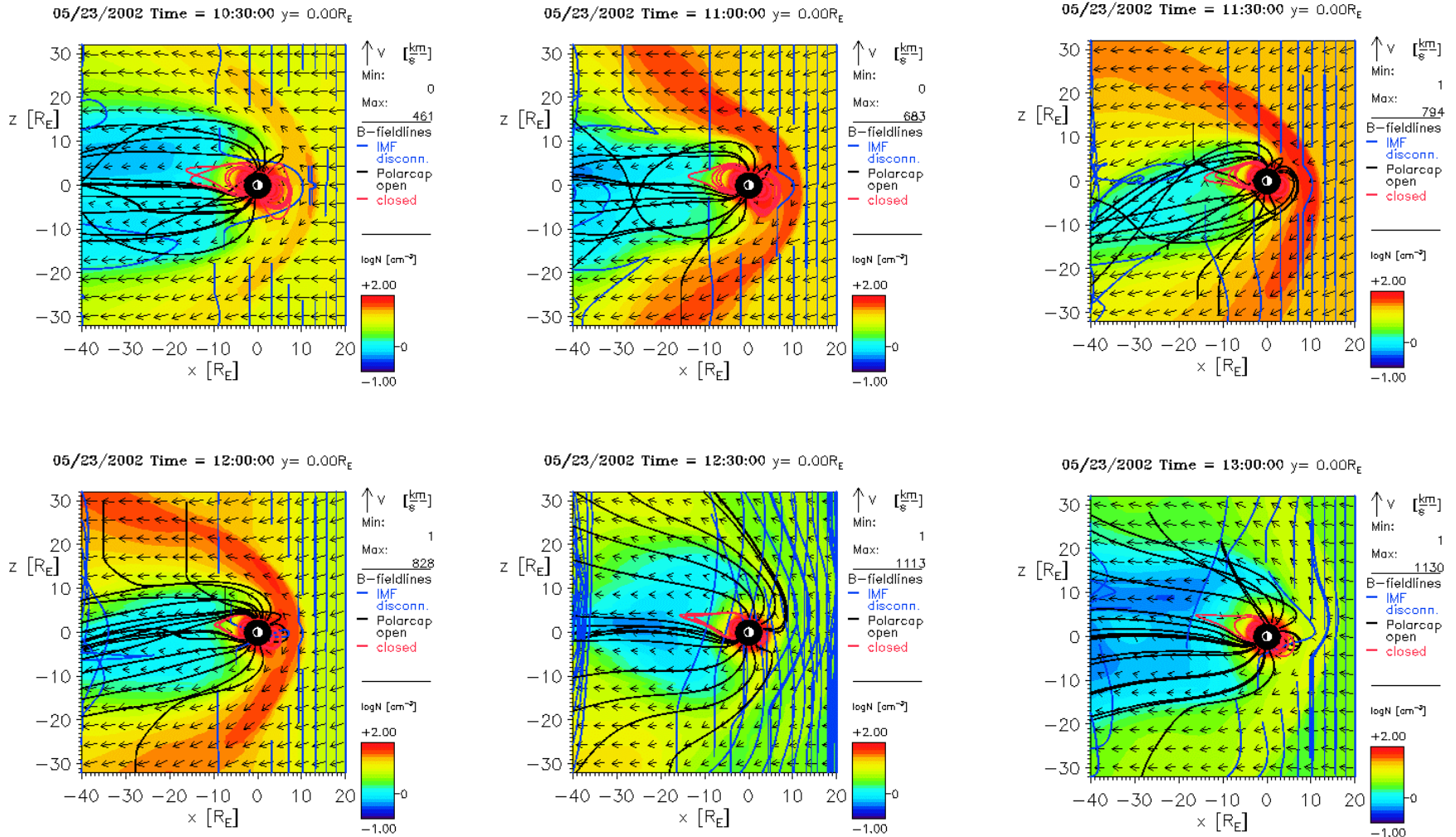


Figure 8

Magnetosphere

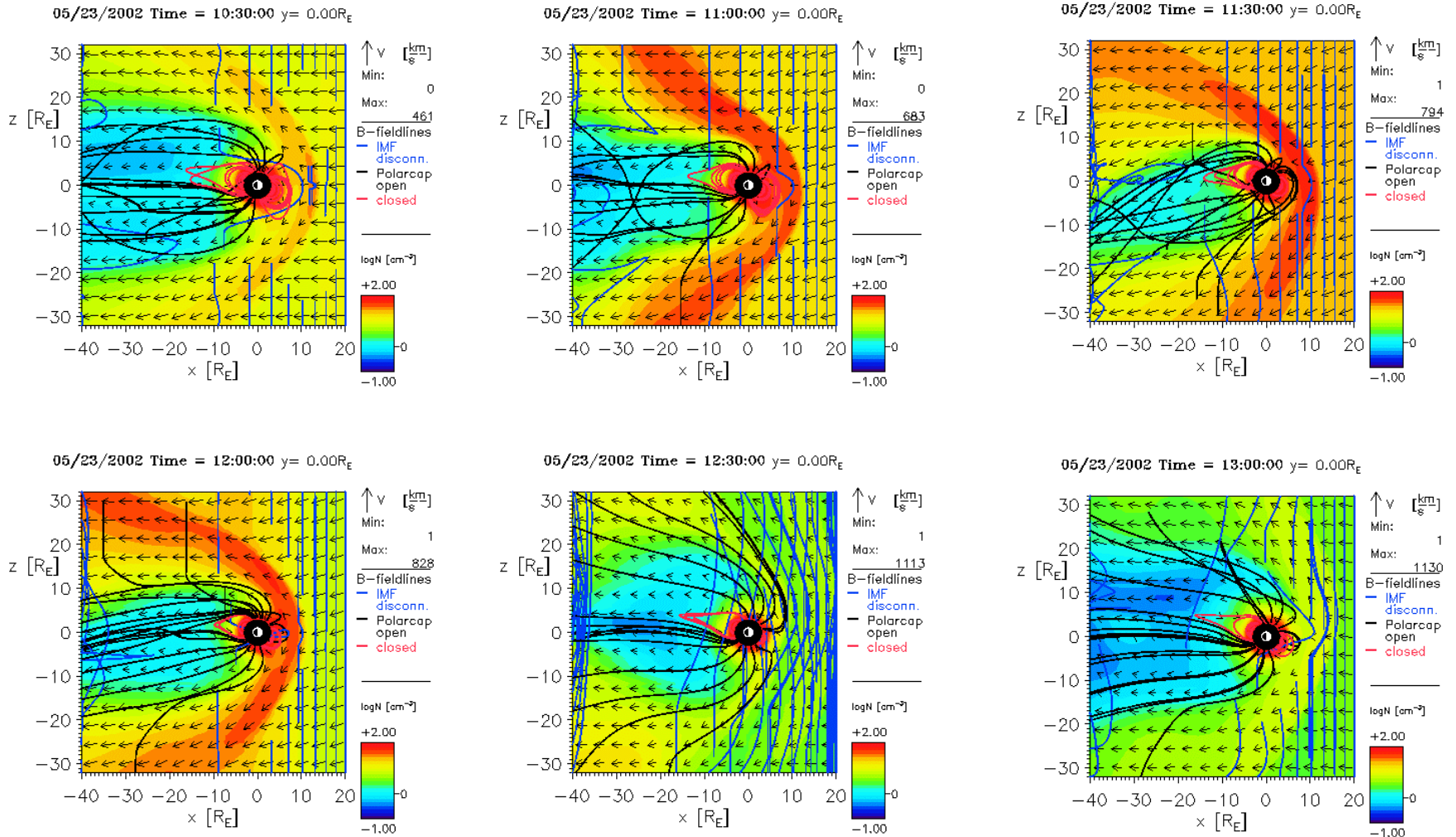


Figure 9

Magnetosphere

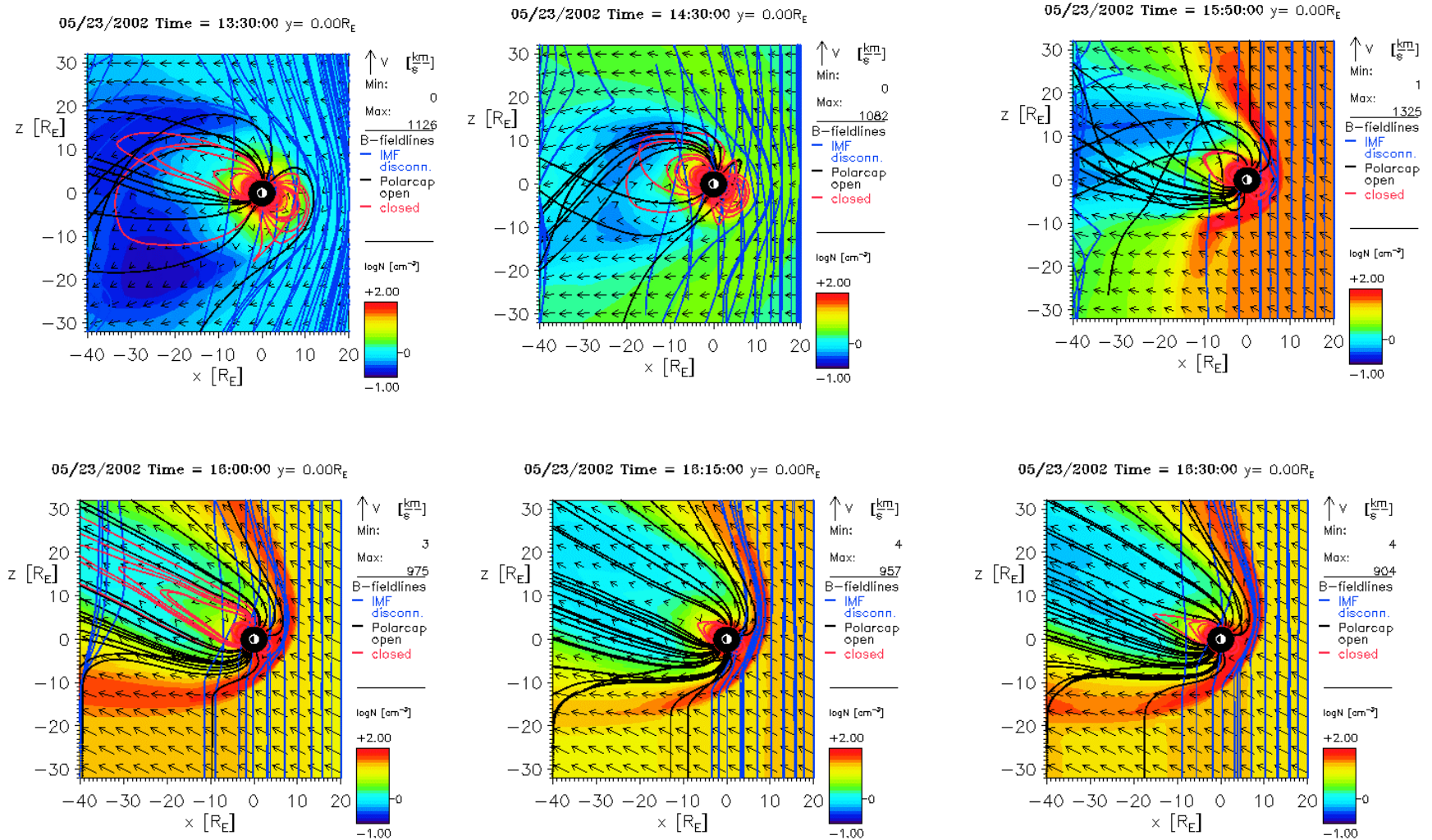


Figure 10

Discussion

- There is a large solar wind density increase between 10:00 and 12:00 (Figure 1). During this time, the magnetosphere compresses and there is a large increase in the cross polar cap potential (Figure 2) followed by an increase in the ring current on the dusk side (Figures 3 and 5). The proton total energy also increases. Increases in the flux can also be seen at geosynchronous orbit around 11:00 for both model and the LANL satellite data (Figure 6 and 7).
- Between 12:00 and 13:00, the solar wind density decreases but the IMF turns southward after 12:10. The cross polar cap potential remains high, the proton total energy increases, and the Dst index decreases. A flux increase is seen around 12:16 on the night side.
- Both the model and the data have similar increases around 11:00, 12:00, and 12:40. The data has sharper increases and decreases than the results from the model. Also the model results show a slightly later timing at 11:00. From 13:00 to 15:30, the model stays relatively flat at geosynchronous orbit while the data stays flat for 3 satellites and decreases for two satellites. The flux is much higher in the model. Around 15:42, there is a flux increase seen in the data that is not seen in the model. There is a flux decrease in the model around 15:48. A second increase is seen around 16:40 for both model and data.

Discussion

- Around 13:15 the IMF turns northward and stays northward for 2.5 hours. The solar wind density is low for this period. The cross polar cap potential is low. Also the proton total energy remains fairly constant from 14:00 to 16:00. The flux at geosynchronous orbit is constant during this time period and the ring current becomes more symmetric.
- After 15:45, the solar wind density increases and the IMF turns southward. The cross polar cap potential increases. The ring current on the night side increases inside geosynchronous orbit. There is a decrease in proton total energy after 16:00 to about 16:12 then the energy increases again till 17:02. The early decrease is when the magnetopause is compressed and there are losses on the dayside. Around 16:12, the flux on the dawnside starts to increase again.

April 17, 2002

Solar Wind Data Propagated to $x = 33 R_E$

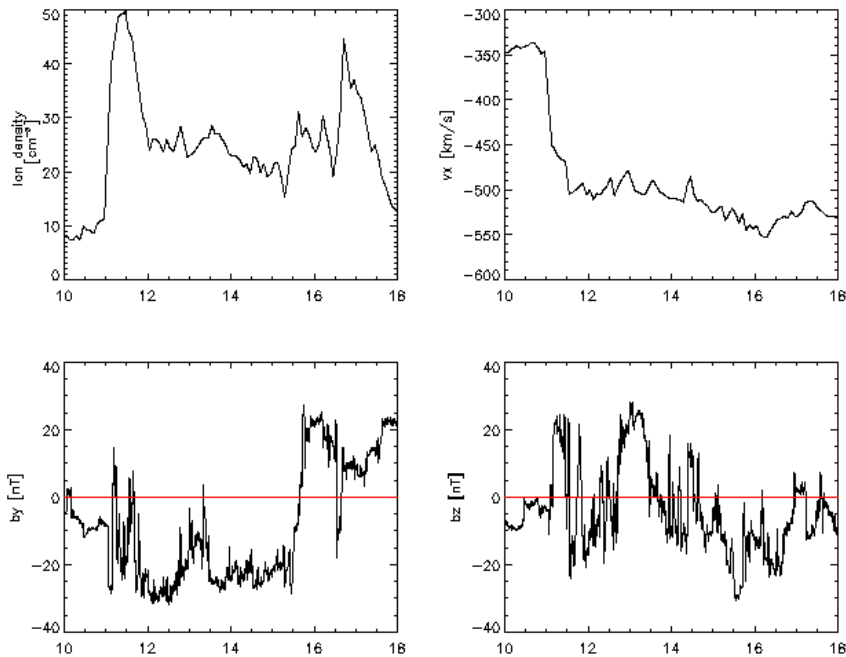


Figure 11

Cross Polar Cap Potential in Northern Hemisphere

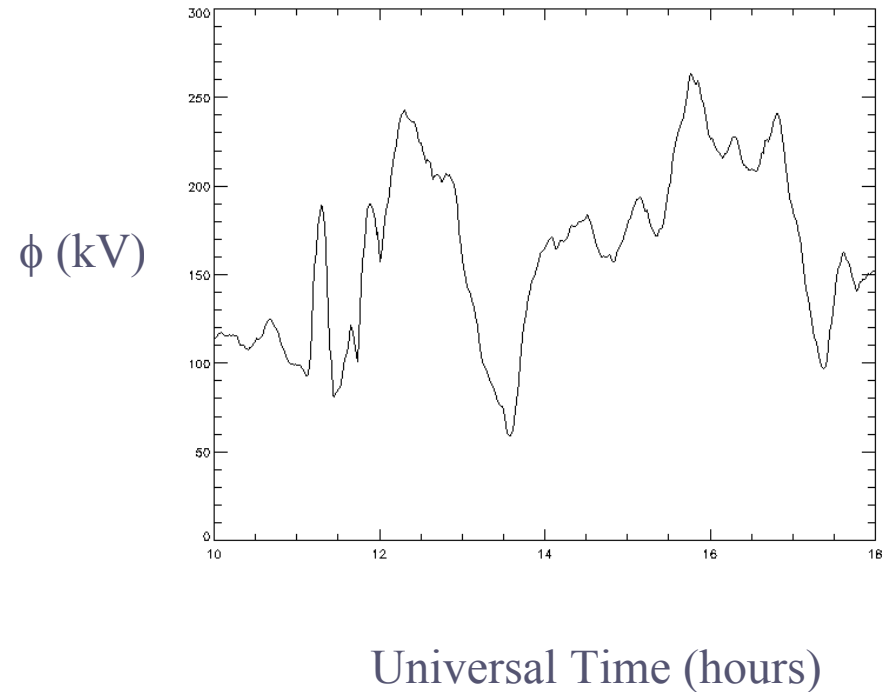


Figure 12

Ring Current

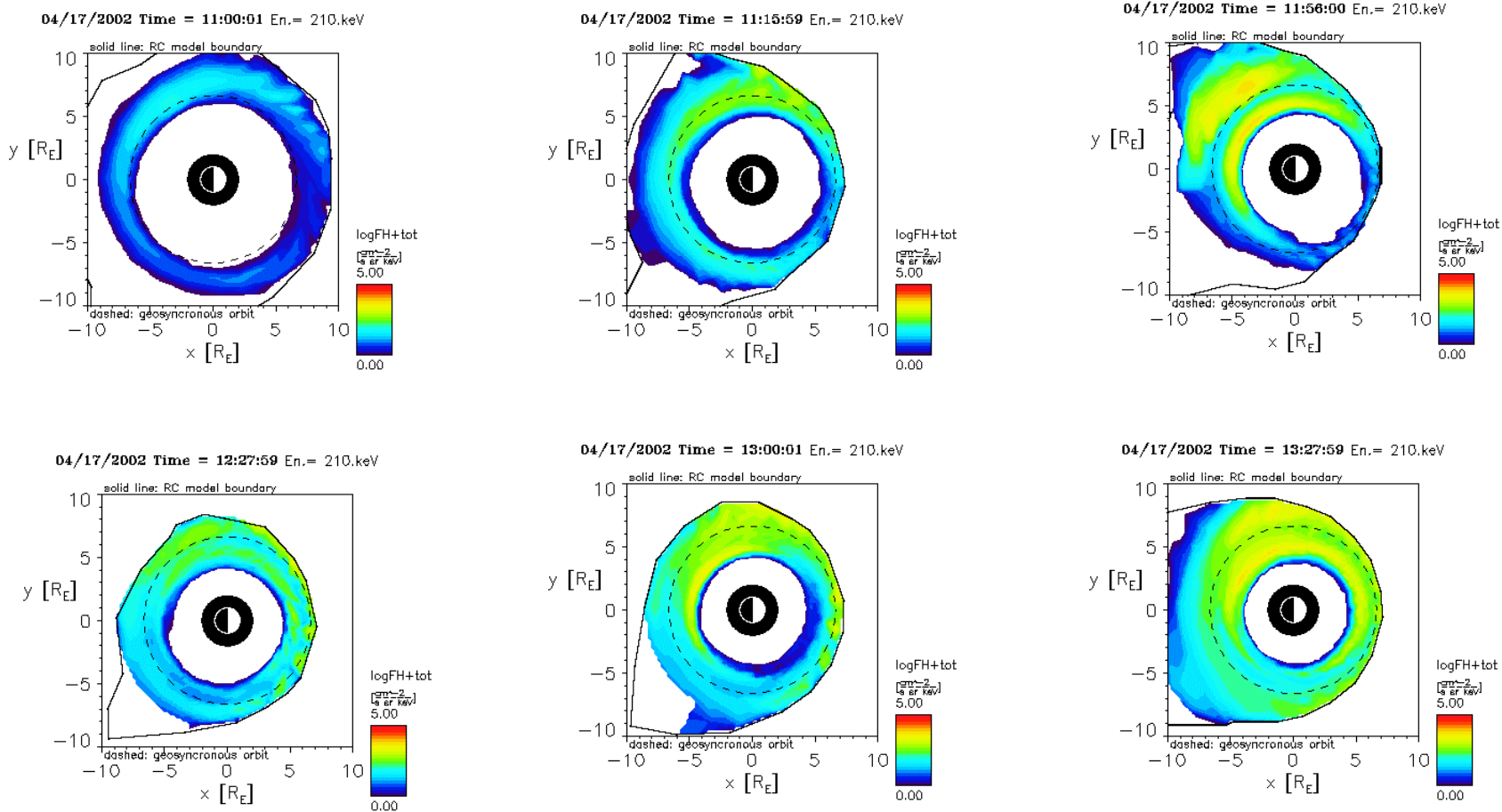


Figure 13

Ring Current

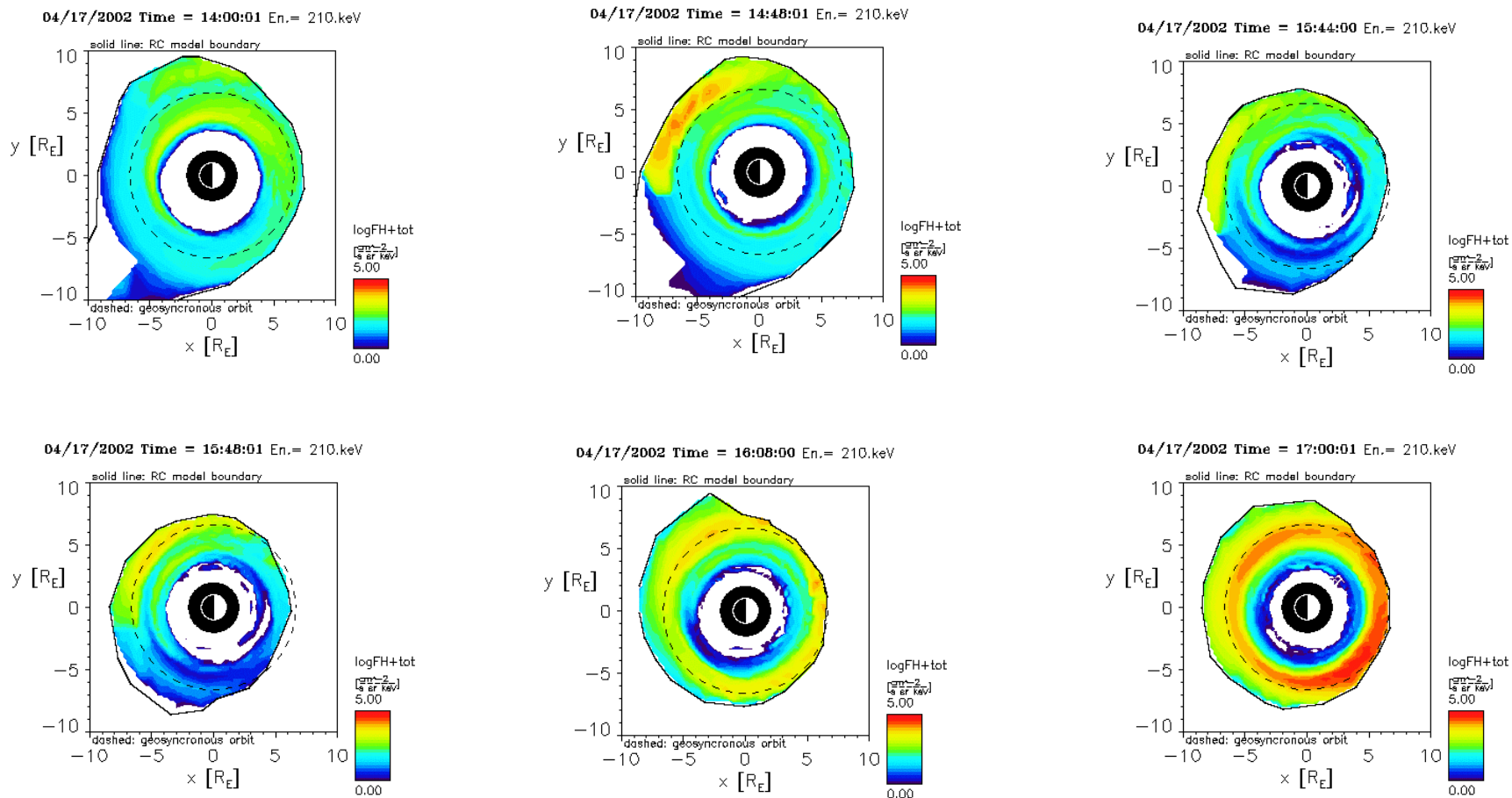


Figure 14

Ring Current

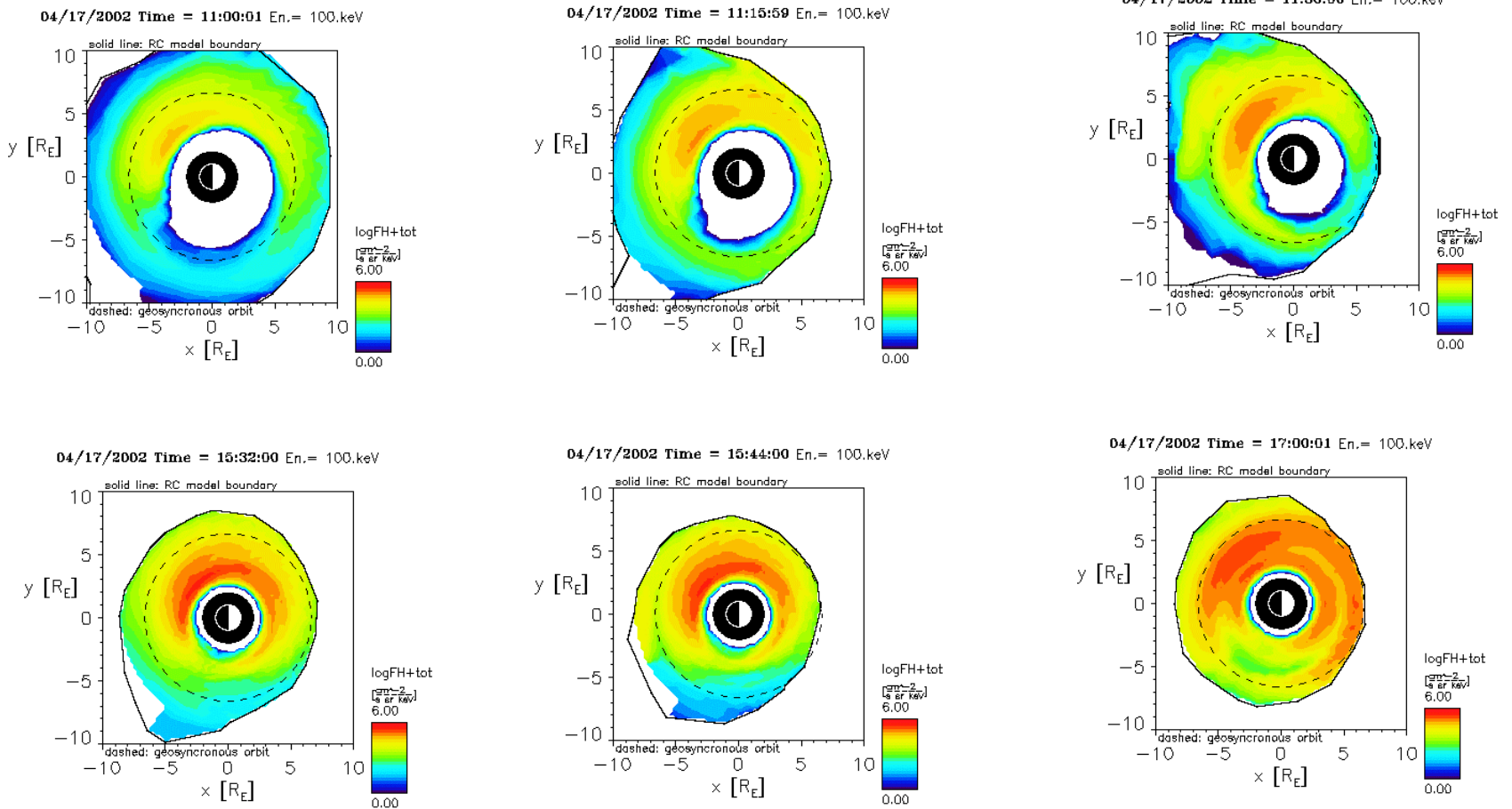


Figure 15

Model Proton Flux

April 17, 2002

Energies (keV):

62.5 black

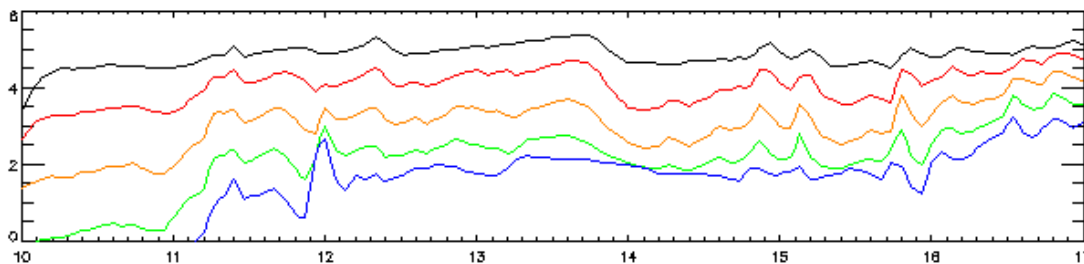
94 red

141.5 orange

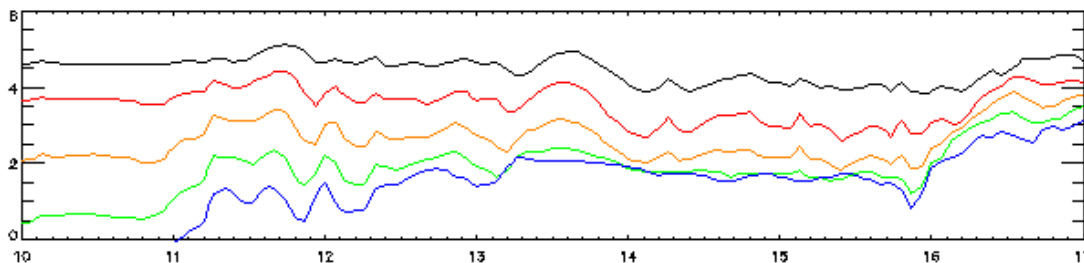
210 green

300 blue

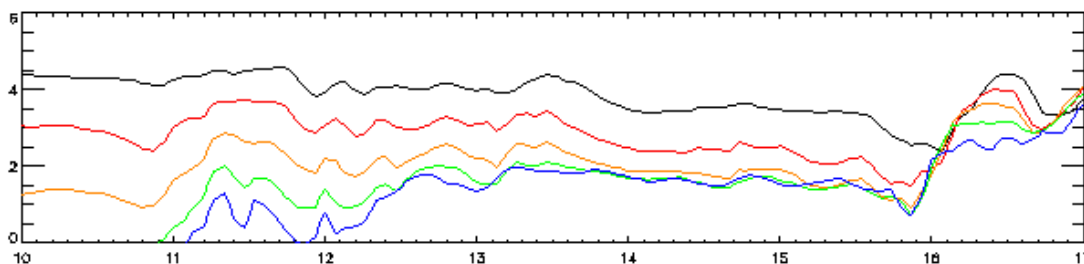
Pitch Angle-Averaged Differential
Flux ($\#/\text{cm}^2/\text{s}/\text{sr}/\text{keV}$)



Magnetic
Longitude
105



Magnetic
Longitude
145



Magnetic
Longitude
-165

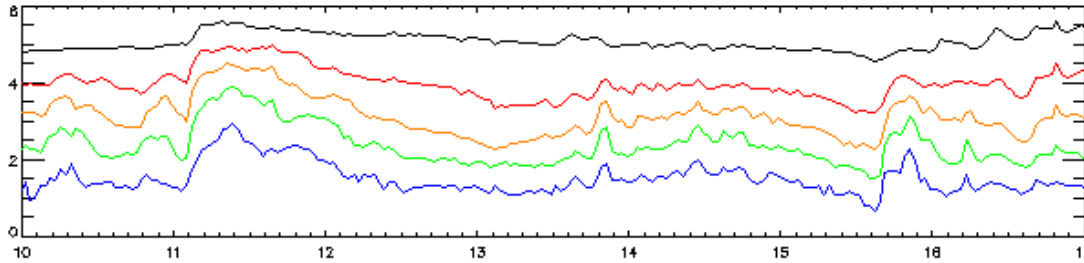
Universal Time (Hours)

Figure 16

LANL Geosynchronous Proton Data

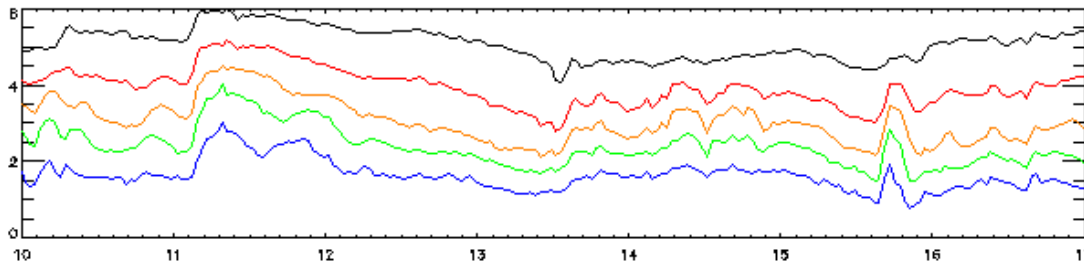
April 17, 2002

Spin-Averaged Differential Flux
(#/cm²/s/sr/keV)



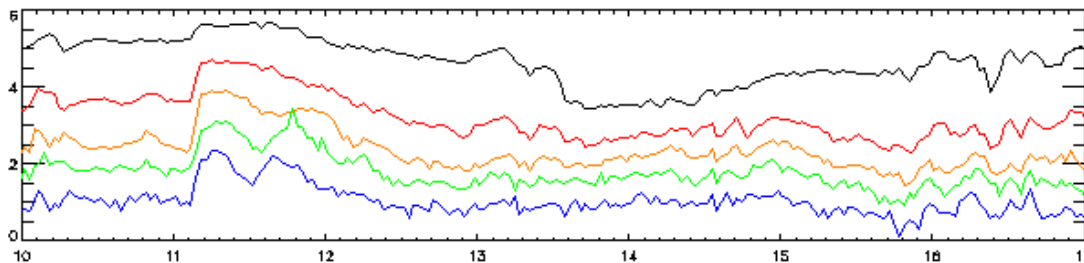
LANL-97A
Geographic
Longitude
104

Energies (keV):
50-75 black



1994-084
Geographic
Longitude
145

75-113 red
113-170 orange
170-250 green
250-400 blue



1991-080
Geographic
Longitude
-165

Universal Time (Hours)

Figure 17

Comparison between LANL data and model

- Both had increases in the flux around 11:12 and 15:40.
- In the LANL data, there were decreases in the flux seen by all three satellites with a minimum around 13:00 for two satellites and 13:30 for the other satellite.
- The model results from orbit calculations did not show a significant decrease. The calculation of the integrated flux showed a decrease but at a later time.

Discussion

- ☛ The shock caused a large compression that increased the density in the magnetosphere and increased the potential in the ionosphere (Figures 11 and 12). The IMF increased and fluctuated in both B_z and B_y . Increases in the proton flux in the model can be seen on the duskside (Figures 13 and 15). Increases in particle fluxes around 11:12 are seen in the LANL data.
- ☛ The increases in the proton flux seen in the model occur mainly with increases in the potential. The flux increase seen at 14:48 does not have a significant potential increase but does have a small increase in the density in the tail.
- ☛ During the time from 11:00 to 14:00, the proton total energy does not increase as much as it did for a similar time period for the May 23 event. Both had similar increases near the end of the run.

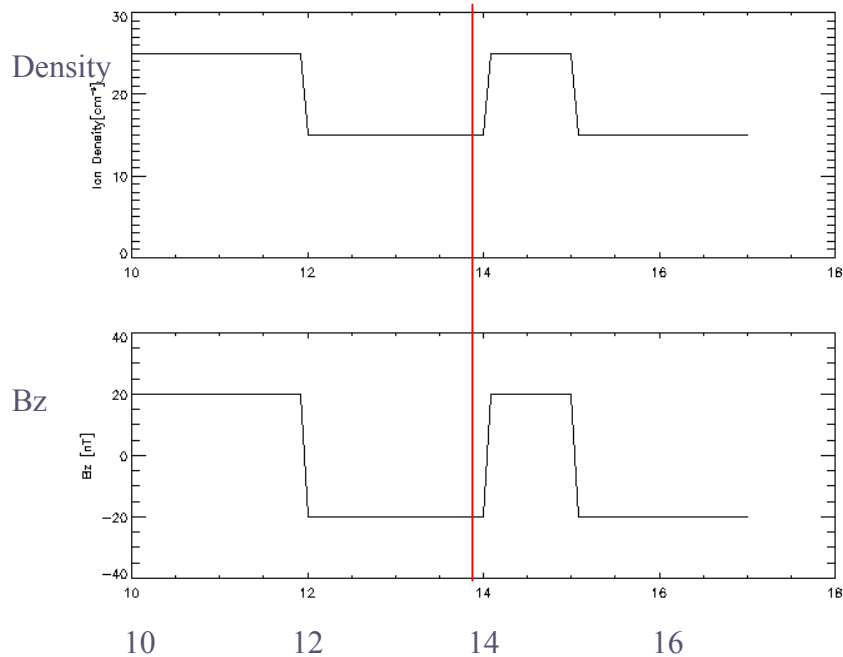
Comparison of May 23 and April 17

- The minimum solar wind density on May 23, 2002 was much lower than on April 17, 2002. Also on April 17, the potential had only one period of low potential. There is significantly more fluctuations in the IMF especially in B_z for April 17 than on May 23.
- For a significant part of the simulation, the ring current was very asymmetric on April 17 as compared to May 23. Significant trapping of particles seems to occur on May 23 during the time of the low potential. For April 17, the proton flux on the dawn side increases after 16:00.
- Also more injections outside geosynchronous orbit are seen for April 17.

Run with Model Solar Wind Conditions

Example 1

Solar Wind Input at 33 R_E



Time in Hours

Figure 18

Cross Polar Cap Potential in Northern Hemisphere

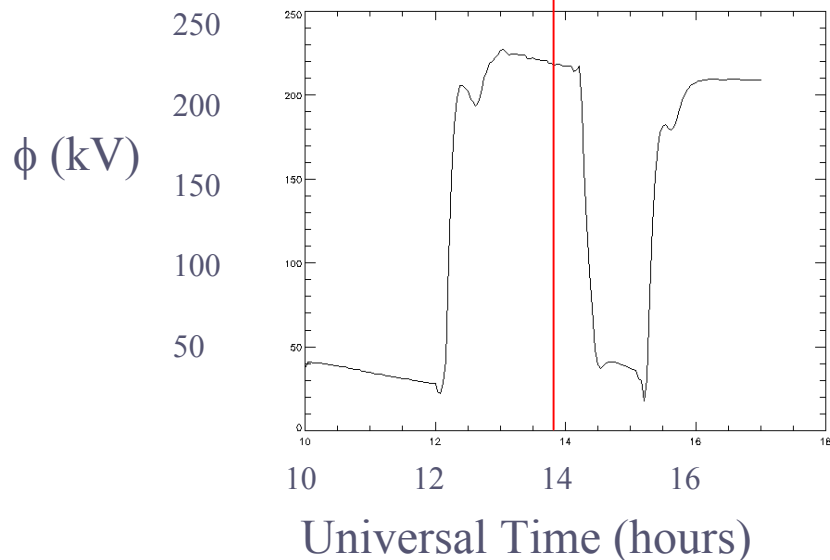


Figure 19

The period before the red line corresponds to a “warm-up” period for the ring current.

Magnetosphere

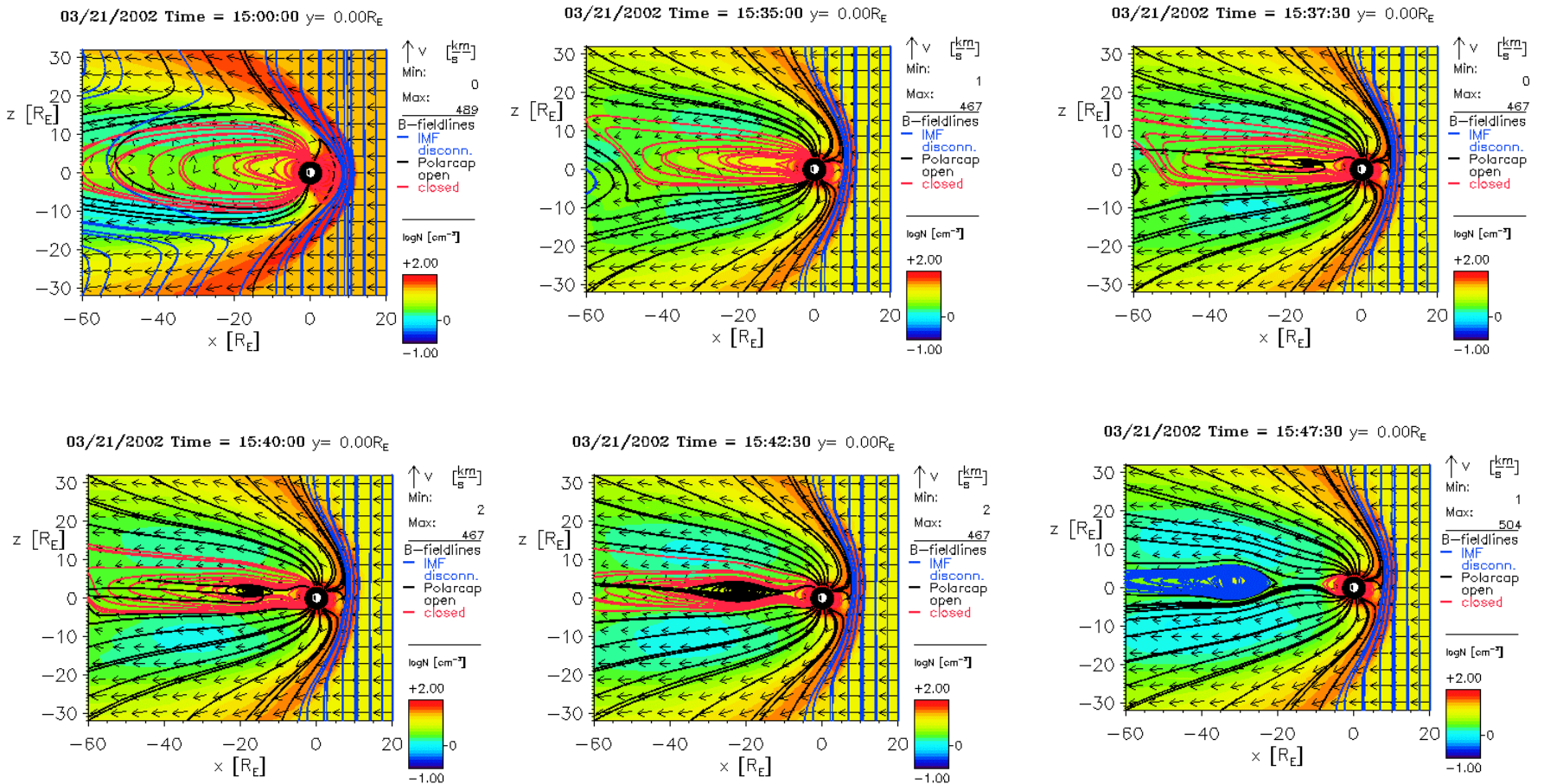
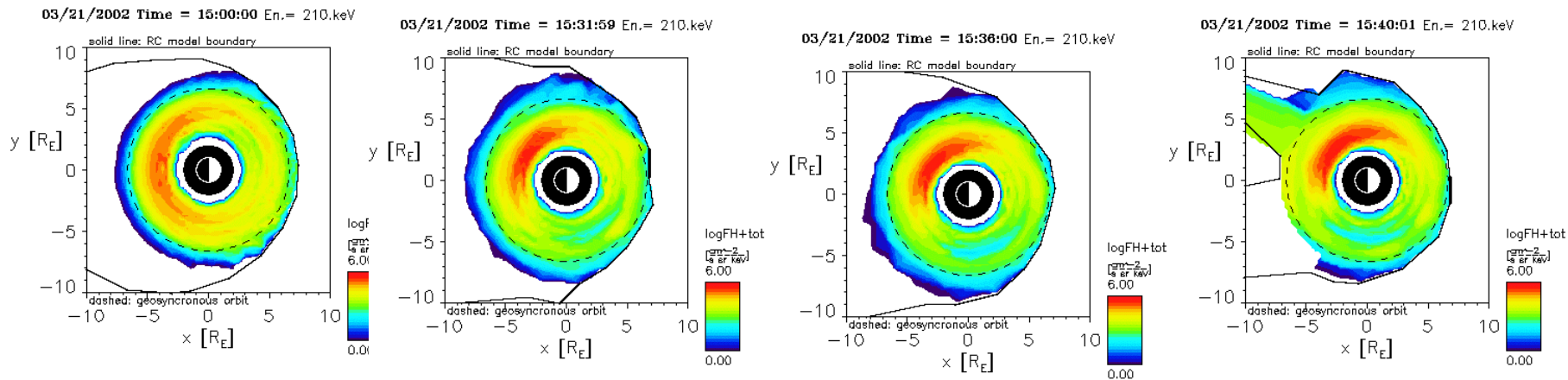


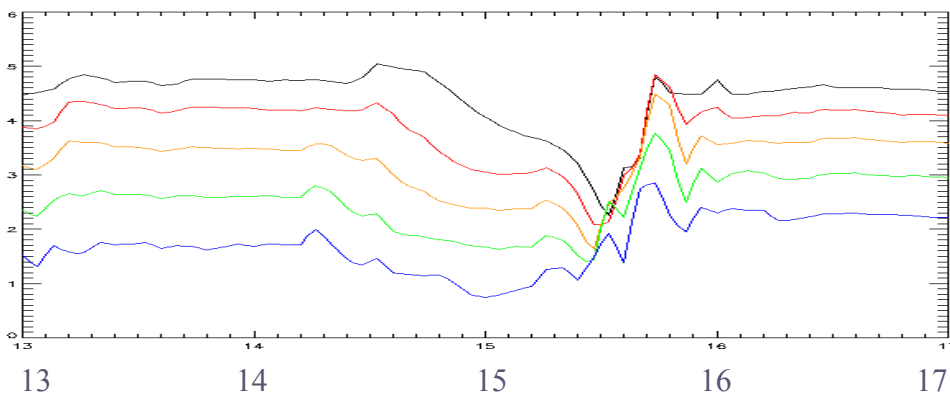
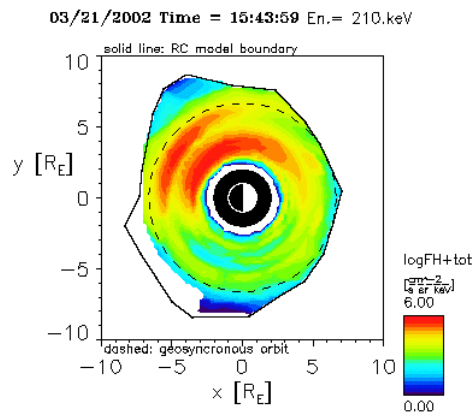
Figure 20

Ring Current



Log (Model Proton Flux) at 21:00 MLT

Energies (keV):



62.5 black

94 red

141.5 orange

210 green

300 blue

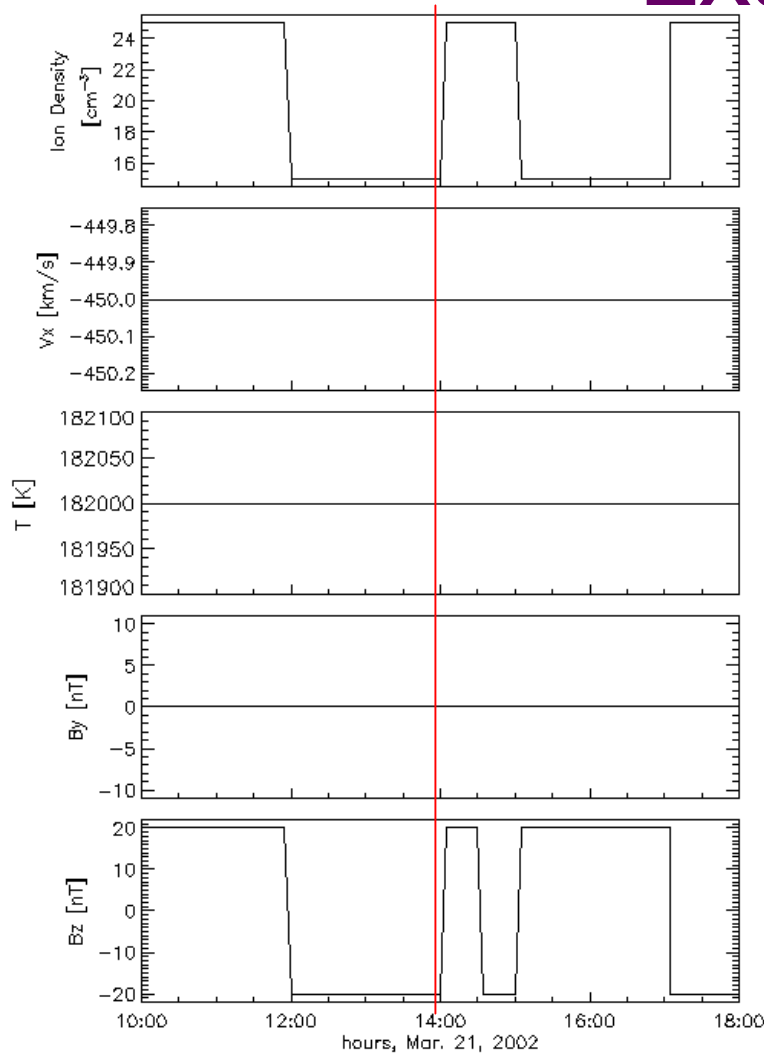
Universal Time (Hours)
Figure 21

Discussion

- ☛ Figure 18 shows the solar wind input. The potential increases as the B_z component turns southward (Figure 19). Figure 24 shows the magnetosphere between 15:00 and 16:00 after the IMF turns southward. During this time, the magnetic field stretches out until 15:35. Around 15:37, reconnection starts.
- ☛ Figure 21 shows the proton flux. After the IMF turns southward, the flux increases inside geosynchronous orbit. After reconnection, there is an injection outside geosynchronous orbit. At geosynchronous orbit (21 MLT), there is an increase in the proton flux when the potential increases. This increase occurs at different times for different energies. There is a sharp increase after reconnection that occurs at approximately the same time for all energies.

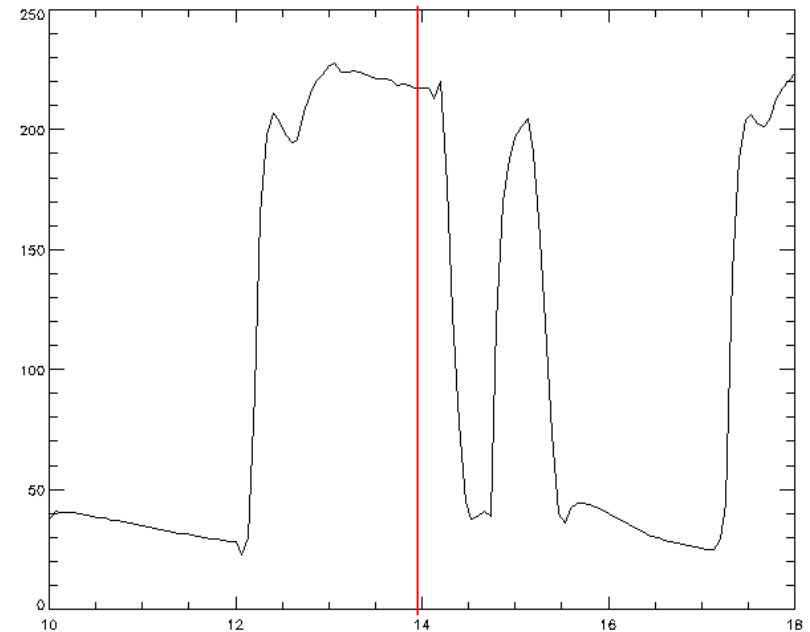
Run with Model Solar Wind Conditions

Example 2



Cross Polar Cap Potential in Northern Hemisphere

ϕ (kV)

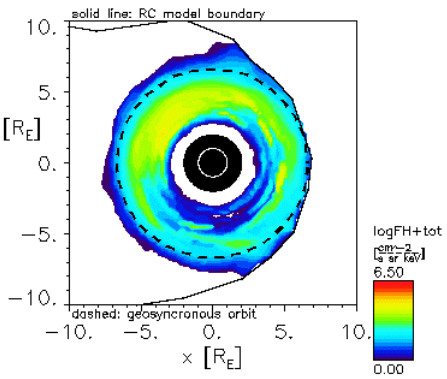


Universal Time (hours)

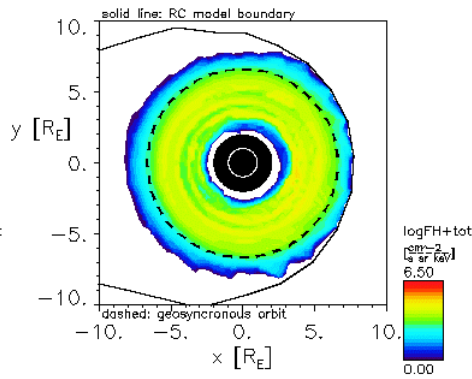
The period before the red line corresponds to a “warm-up” period for the ring current.

Ring Current

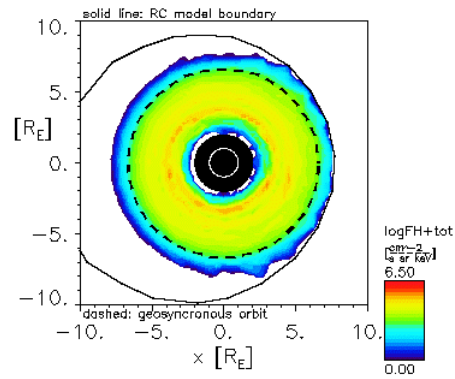
03/21/2002 Time = 15:00:00 En.= 300.keV



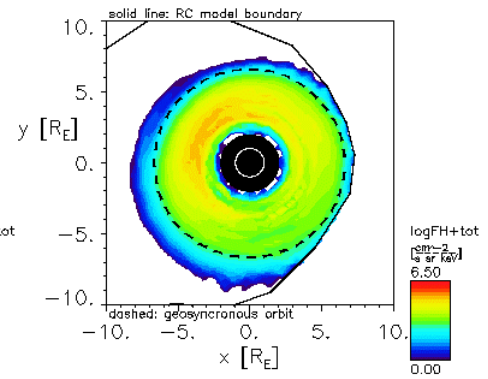
03/21/2002 Time = 16:04:01 En.= 300.keV



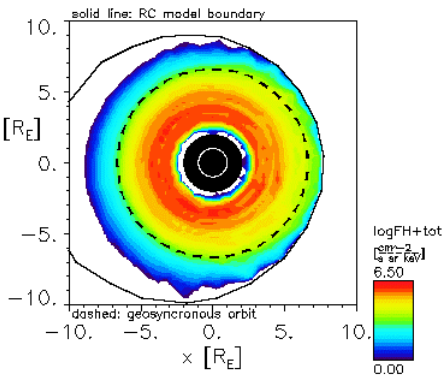
03/21/2002 Time = 17:00:00 En.= 300.keV



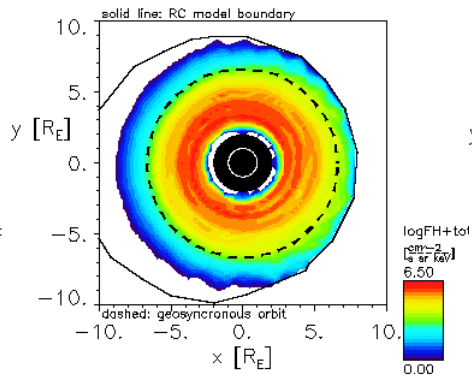
03/21/2002 Time = 17:28:01 En.= 300.keV



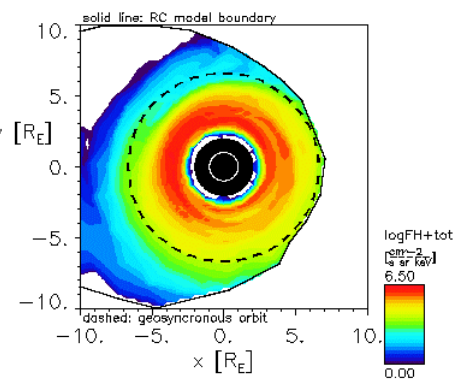
03/21/2002 Time = 17:00:00 En.= 150.keV



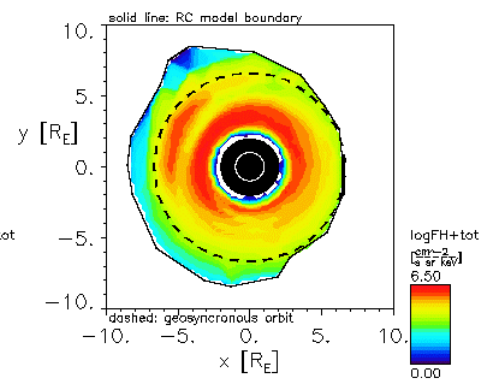
03/21/2002 Time = 17:19:59 En.= 150.keV



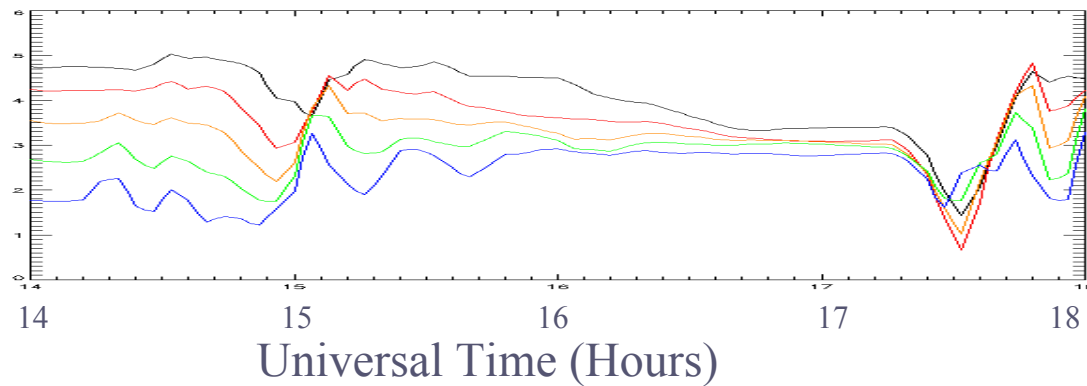
03/21/2002 Time = 17:38:00 En.= 150.keV



03/21/2002 Time = 17:48:00 En.= 150.keV



Log (Model Proton Flux) at 21:00 MLT



Energies (keV):

62.5 black

94 red

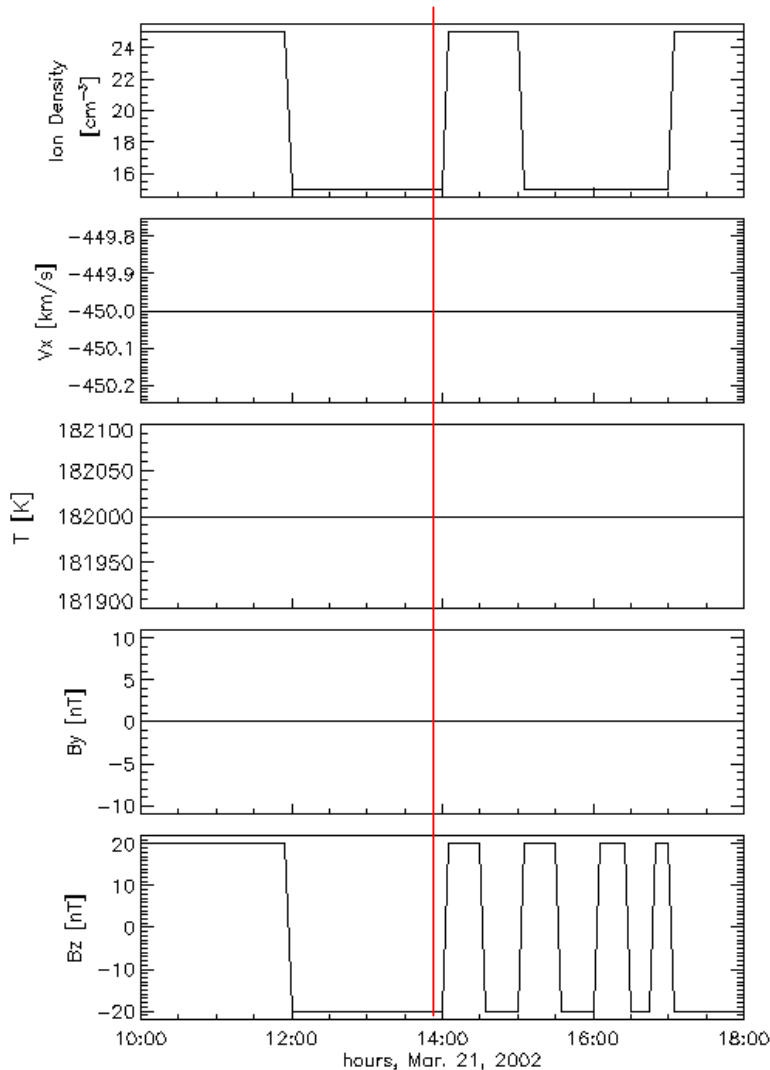
141.5 orange

210 green

300 blue

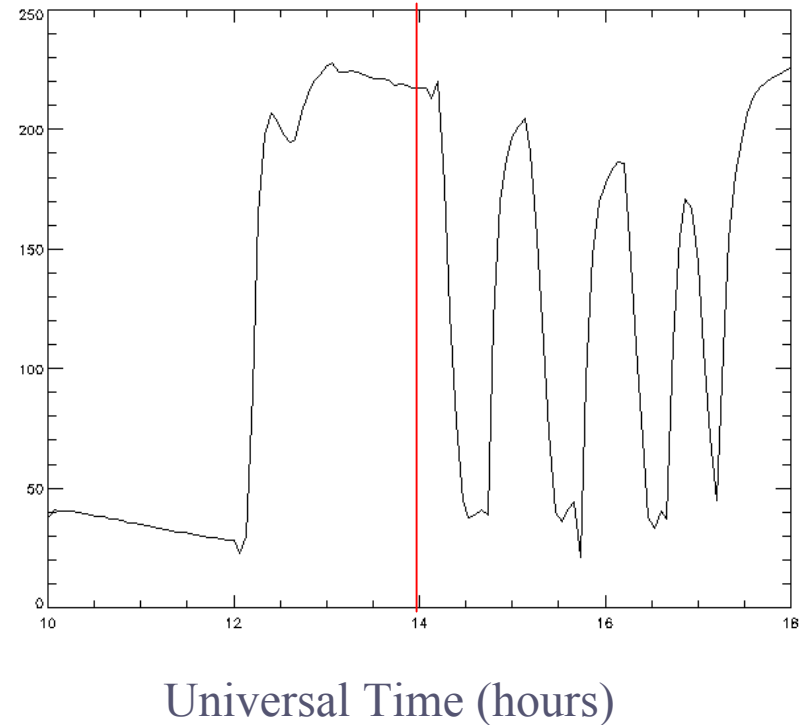
Run with Model Solar Wind Conditions

Example 3



Cross Polar Cap Potential in Northern Hemisphere

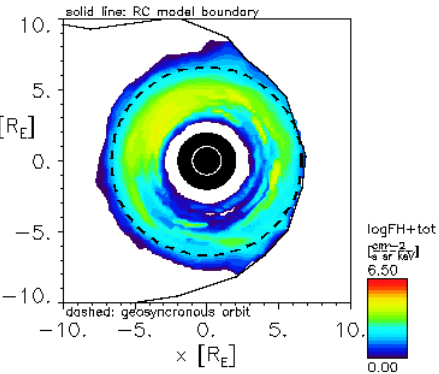
ϕ (kV)



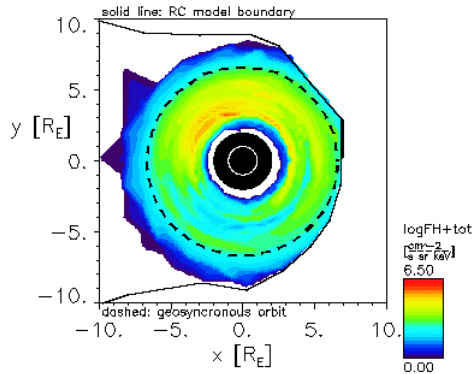
The period before the red line corresponds to a “warm-up” period for the ring current.

Ring Current

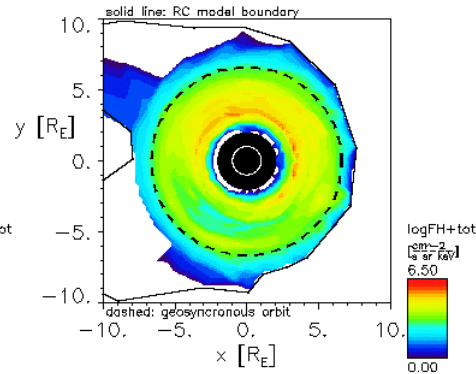
03/21/2002 Time = 15:00:00 En.= 300.keV



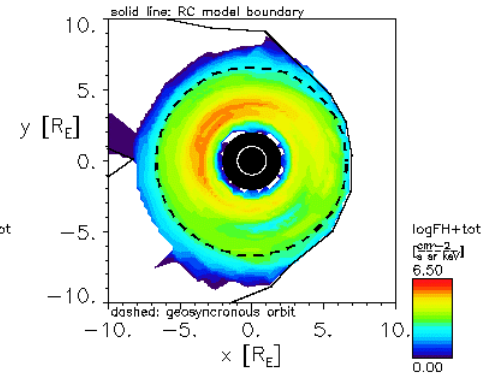
03/21/2002 Time = 16:04:01 En.= 300.keV



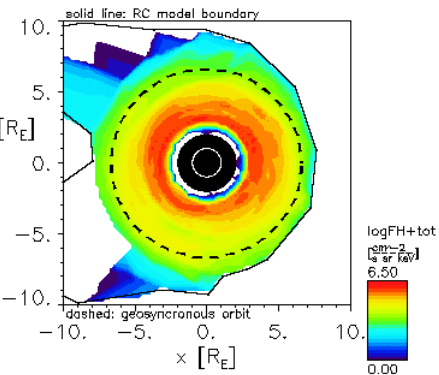
03/21/2002 Time = 17:00:00 En.= 300.keV



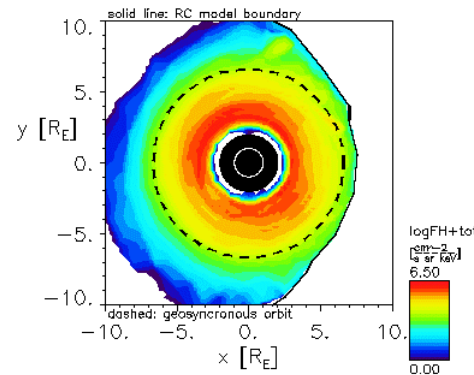
03/21/2002 Time = 17:28:01 En.= 300.keV



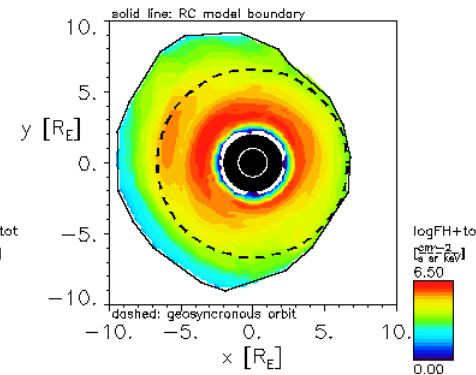
03/21/2002 Time = 17:00:00 En.= 150.keV



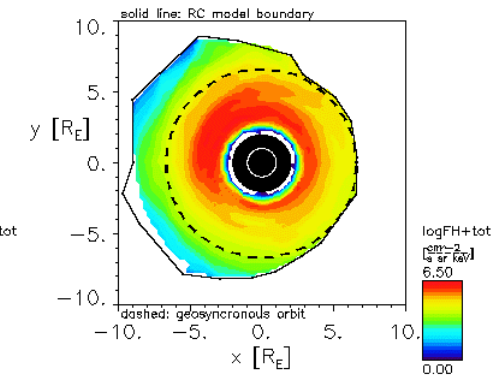
03/21/2002 Time = 17:19:59 En.= 150.keV



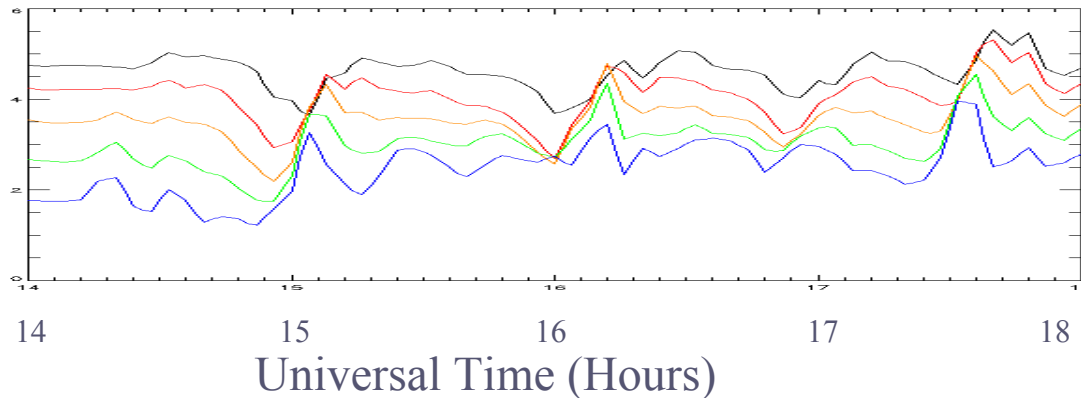
03/21/2002 Time = 17:36:00 En.= 150.keV



03/21/2002 Time = 17:48:00 En.= 150.keV



Log (Model Proton Flux) at 21:00 MLT



Energies (keV):

62.5 black

94 red

141.5 orange

210 green

300 blue

Discussion

- In example 2, the higher energy fluxes become symmetric between 15:00 and 17:00. This is similar to the May 23, 2002 event. Both cases had a 2-hour period of low solar wind density and northward IMF. This allows more trapping of particles since there is smaller dayside losses. Radial diffusion is probably significant for the higher energies inside geosynchronous orbit.
- In example 3, the run is not as symmetric as example 2. In this case the IMF is fluctuating between north and south similar to the April 17, 2002 event. The April 17, 2002 is more asymmetric than example 3 probably due to the higher solar wind density compressing the magnetosphere more and allowing more losses at the dayside magnetopause.
- In example 2 after the IMF turns southward, there is a flux dropout in the pre-midnight sector (especially in the 90-150 keV energy range). The flux dropout at high energies during growth phase is due to B decrease at this substorm phase. In order to conserve the third adiabatic invariant, ions drift shells expand to higher L and at the same time particles lose energy. This causes the flux dropout. In example 3, there is no large flux dropout.

References

- Powell K. G., P. L. Roe, T. J. Linde, T. I. Gombosi, and D. L. De Zeeuw, A solution-adaptive upwind scheme for ideal magnetohydrodynamics, *J. Comput. Phys.*, 154(2), 284-309, 1999.
- Fok M.-C., T. E. Moore, and M. E. Greenspan, Ring current development during storm main phase, *J. Geophys. Res.*, 101, 15,311-15,322, 1996.

Acknowledgments

- This work was performed while one of the authors (K.A.K) held a National Research Council Research Associateship at Goddard Space Flight Center.
- Geosynchronous proton flux data was provided by the Energetic Particle team at Los Alamos National Laboratory, Richard Belian (PI).
- ACE data was obtained through the CDAWeb. We thank the ACE SWEPAM instrument team and the ACE MAG instrument team for the data.